Biosensors and Bioelectronics 134 (2019) 103–108

Contents lists available at ScienceDirect

Biosensors and Bioelectronics

journal homepage: www.elsevier.com/locate/bios

Binding-induced formation of DNAzyme on an Au@Ag nanoparticles/TiO_2 nanorods electrode: Stimulating biocatalytic precipitation amplification for plasmonic photoelectrochemical bioanalysis

Ling Zhang[a,b,c,1], Xiao-Mei Shi[a,1], Yi-Tong Xu[a], Gao-Chao Fan[b], Xiao-Dong Yu[a,*], Yan-Yu Liang[c,**], Wei-Wei Zhao[a,***]

[a] State Key Laboratory of Analytical Chemistry for Life Science, School of Chemistry and Chemical Engineering, Nanjing University, Nanjing, 210023, China
[b] Shandong Key Laboratory of Biochemical Analysis, College of Chemistry and Molecular Engineering, Qingdao University of Science and Technology, Qingdao, 266042, PR China
[c] School of Materials Science and Technology, Nanjing University of Aeronautics and Astronautics, Nanjing, 211106, China

ARTICLE INFO

Keywords:
Photoelectrochemical
Bioanalysis
Hairpin DNA
DNAzyme
Precipitation

ABSTRACT

Photoelectrochemical (PEC) DNA bioanalysis has been drawing more attention in recent years due to the advantages of PEC technique and the vital importance of DNA biomolecules. DNAzymes are unique catalytic nucleic acid molecules that are capable of catalyzing specific biochemical reactions. Using the target-binding-induced conformation change of hairpin DNA probe to hemin/G-quadruplex-based DNAzyme and a plasmonic Au@Ag nanoparticles (NPs)/TiO_2 nanorods (NRs)/fluorine-doped tin oxide (FTO) heterostructured photoelectrode, this work reported a novel and sensitive PEC DNA analysis on the basis of a DNAzyme-stimulated biocatalytic precipitation (BCP) strategy. In such a design, the BCP-induced decrease of plasmonic photocurrent can be related to the target-responsive formation of DNAzymes and thus be monitored to assay the target DNA from 0.1 and 100 nM. In brief, with a plasmonic photoelectrode and a hairpin probe, this work reported a general plasmonic DNAzyme-based PEC DNA analysis, which could also be easily extended to aptasensing toward numerous targets of interest.

1. Introduction

Photoelectrochemical (PEC) analysis has been widely used in environmental analysis and life analysis due to the advantages of simple instrument, easy miniaturization, rapid response, and low cost (Zhao et al., 2017; Tu et al., 2018). It shows good performance in pesticide residue detection (Song et al., 2018a), pollution detection (Kang et al., 2010; Xu et al., 2018a; Peng et al., 2018a), ion detection (Li et al., 2018a; Shi et al., 2018a), DNA detection (Peng et al., 2018b; Zhang et al., 2018a), immunoassay (Zhang et al., 2018b; Kong et al., 2018; Qileng et al., 2018), enzyme detection (Cui et al., 2018; Song et al., 2018b; Shi et al., 2018b), cell analysis (Ding et al., 2016) and so on. Nucleic acids (DNA and RNA) are important biomolecules, the accurate and sensitive analysis of nucleic acids is crucial for early diagnosis and treatment of fatal diseases. PEC DNA/RNA analysis has been drawing more attention in recent years as demonstrated by increasing research articles. For example, Zhu et al. reported a PEC biosensor for DNA detection by terminal deoxynucleotidyl transferase-mediated extension and enzymatic signal amplification (Shen et al., 2015). Zang et al. developed a PEC biosensor for DNA assays using catalytic hairpin assembly and mimetic enzyme signal amplification (Zang et al., 2015).

Signal amplification is essential for ultrasensitive PEC bioanalysis. Among various strategies, biocatalytic precipitation (BCP), taking advantage of the formation of an insoluble layer on the electrode surface, is a simple and convenient strategy. The buildup of BCP on the photoelectrode could alter the interfacial electron-transfer property and obviously impair the photocurrent signaling. Previously, protein enzymes have been introduced to generate BCP for specific PEC immunoassays. For example, based on the oxidation of 4-chloro-1-naphthol (4-CN) by H_2O_2 to produce insoluble product benzo-4-

* Corresponding author.
** Corresponding author.
*** Corresponding author.
E-mail addresses: yuxd@nju.edu.cn (X.-D. Yu), liangyy403@126.com (Y.-Y. Liang), zww@nju.edu.cn (W.-W. Zhao).
[1] These authors contributed equally to this work.

https://doi.org/10.1016/j.bios.2019.03.059
Received 6 December 2018; Received in revised form 25 March 2019; Accepted 26 March 2019
Available online 30 March 2019
0956-5663/

chlorohexadienone in the presence of horseradish peroxidase (HRP), an ultrasensitive sandwich PEC detection of mouse IgG protocol had been established (Zhao et al., 2012). In addition, alkalinephosphate (ALP) could catalyze the oxidative hydrolyzing transformation of 5-bromo-4-chloro-3-indoyl phosphate (BCIP) to yield an indigo precipitation on the surface of the electrode, resulting in the suppression of the photocurrent responses (Zhang et al., 2016a, 2018c). Nanoenzymes have also been exploited to BCP-based PEC immunoassay (Gong et al., 2016). DNAzymes are catalytic nucleic acid molecules that are capable of catalyzing specific biochemical reactions. With such a DNAzyme-based BCP strategy, some recent works reported the PEC analysis of polynucleotide kinase activity (Zhuang et al., 2015), mouse IgG (Wang et al., 2015), and CEA (Ge et al., 2016), respectively.

To allow the BCP-based signaling, proper photoelectrodes with strong photocurrent responses are essential. Heterostructures with high photoelectric conversion efficiency have been considered as ideal candidates for the development of photoelectrode due to their unique structural and functional characteristics. It is believed that such a structure could integrate different properties of the individual components and thus achieve enhanced properties. With TiO_2 nanostructures for example, one effective strategy is to combine TiO_2 with various chalcogenide semiconducting species, such as CdS (Karuturi et al., 2018), CdSe (Nehme et al., 2016), Ag_2S (Ghafoor et al., 2017), PbS (Pathak et al., 2018; Li et al., 2015; Zhang et al., 2016b), Bi_2S_3 (Li et al., 2018b; Kulkarni et al., 2016), $CuInS_2$ (Xu et al., 2018b; Gao et al., 2018) and so on. Due to the sensitization effect, the recombination probability of the photogenerated charge carriers is reduced, resulting in enhanced photoelectric conversion efficiency. Significantly, another strategy is to combine TiO_2 with noble metal nanoparticles (NPs) with surface plasmon resonance (SPR) properties (Liu et al., 2018a; Wang et al., 2018; Chen et al., 2018; Zhou et al., 2018; Da et al., 2014). The SPR-enhanced energy conversion is mainly attributed to the electrical field amplification effect as well as the injection of SPR-generated hot electrons into the conduction band of TiO_2. For example, the ALP tagged antibodies on Au NPs/TiO_2 nanotubes electrode has been used for plasmonic PEC immunoassay (Zhu et al., 2016). Compared with Au NPs, Ag NPs have a wider absorption range, and the optical absorption range can be wider when it is combined with TiO_2. For example, Ag decorated TiO_2/sepiolite showed greatly enhanced photocatalytic activity in the photocatalytic degradation of methyl orange under UV–vis light irradiation (Liu et al., 2018b). Therefore, combining plasma effect of Ag NPs with TiO_2 would potentially present a good plasmonic photoelectrode for BCP-based PEC bioanalysis application.

Herein, using an Au@Ag NPs/TiO_2 nanorods (NRs)/fluorine-doped tin oxide (FTO) heterostructured photoelectrode, we report a novel and sensitive PEC DNA analysis on the basis of binding-induced conformation change from hairpin DNA probe to hemin/G-quadruplex-based DNAzyme and its catalytic generation of precipitation product for signal amplification. Specifically, as shown in Scheme 1, TiO_2 NRs arrays were prepared on FTO glass using a hydrothermal method (Liu and Aydil, 2009), while the Au@Ag NPs was synthesized by sequential formation of Au NPs and Ag layer (Zeng et al., 2018). After modification of the Au@Ag NPs onto the TiO_2 NRs/FTO electrode through the mediation of poly (diallyldimethylammonium chloride) (PDDA), hairpin DNA (hDNA) probe was anchored onto the electrode for the recognition of target DNA (tDNA) in the sample. The formation of resultant dual stranded DNA (dsDNA) which would open the hDNA probe and form G-tetrad, which will further form DNAzymes in the presence of hemin. The hemin/G-quadruplex-based DNAzyme can catalyze the oxidation of 4-chloro-1-naphthol (4-CN) by hydrogen peroxide and generate precipitate of benzo-4-chlorohexadienone on the electrode surface. The decrease of plasmonic photocurrent can thus be monitored to assay the target DNA. Using a plasmonic photoelectrode and a hairpin probe, this work reported a general plasmonic DNAzyme-based PEC DNA analysis, which could also be easily extended to aptasensing toward numerous targets of interest and to our knowledge has not been reported. The detailed fabrication, characterization, and performance of the developed PEC DNA biosensor are described below.

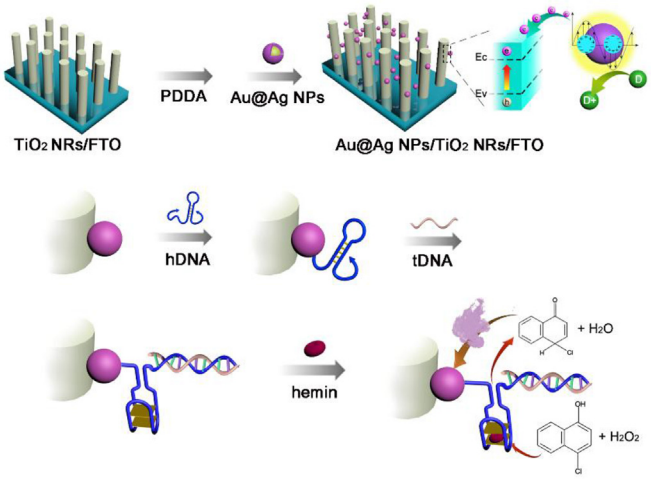

Scheme 1. Preparation and operation principle of the plasmonic DNAzyme-based PEC bioanalysis.

2. Experimental section

2.1. Reagents and apparatus

Poly (diallyldimethylammonium chloride) (PDDA, 20%, w/w in water, MW = 200 000–350 000), 1-Ethyl-3-(3-dimethylaminopropyl) carbodiimide (EDC), N-Hydroxysuccinimide (NHS), and monoethanolamine (MEA) were supplied from Sigma-Aldrich, (St. Louis, MO). Ascorbic acid (AA), isopropanol, titanium tetrachloride, acetone, silver nitrate, ammonia (25%–28%), formaldehyde, sodium citrate, sodium hydroxide, auric chloride acid ($HAuCl_4$) , hydrochloric acid, hemin, and thioglycollic acid (TGA) were supplied from Sinopharm Chemical Reagent Co., Ltd (China). Titanium tetrachloride, 4-chloro-1-naphthol (4-CN), acetone, silver nitrate, ammonia (25%–28%), and formaldehyde were supplied from Nanjing Chemical Reagent Co., Ltd. The fluorine-doped tin oxide (FTO) glass (type with FTO coating 180 ± 20 nm, sheet resistance 14 Ω cm^{-2}) was obtained from Wuhan Ge-Ao Ltd., Wuhan, China. Ultrapure water (18.2 MΩ cm resistivity at 25 °C, Millier Q) was used in all experiments. The synthetic oligonucleotides with the following seqences were purchased from Nanjing GenScript Biotech Corp: hDNA: 5′-AAGGGTTGGGCGGGATGGGTTACC TCAGTGCTTATTCGAAACCCA-3′, (5′ Amino Modified), complementary matched tDNA (CMM): 5′-TCGAATAAGCACTGAGGT-3′, double-base mismatched DNA (DMM): 5′-TCGAACAAGCACCGAGGT-3′, four-base mismatched DNA (FMM): 5′-TCGCATACGCATTGAGTT-3′, non-complementary matched DNA (NCMM): 5′-ATCCTATTAGTTCATATC-3’.

SEM images were recorded by a Hitachi S4800 scanning electron microscope (Hitachi Co., Japan). XPS was obtained from PHI 5000 VersaProbe (UlVAC-PHI Co., Japan). The UV–vis absorption spectra and UV–vis diffuse reflectance spectra were obtained on a Shimadzu UV-3600 UV–vis–NIR spectrophotometer (Shimadzu Co., Japan). XRD spectra were characterized by powder X-ray diffraction (XRD) [X'TRA, Cu Kα (ARL Co.)]. PEC measurements were performed with a home-made PEC system equipped with a 5 W light-emitting diode lamp emitting visible light with a power density of 1.6 mW/cm^2. The photocurrent was measured on a CHI 660C electrochemical workstation with a three-electrode system: a Au@Ag NPs/TiO_2 NRs/FTO electrode with a geometrical circular area (0.5 cm in diameter) as the working electrode, a Pt wire as the counter electrode, and a Ag/AgCl electrode as the reference electrode. The photocurrent measurements were taken at a constant potential of 0.0 V (vs Ag/AgCl), and 0.1 M AA phosphate buffer (pH 7.4) was used as the supporting electrolyte for photocurrent

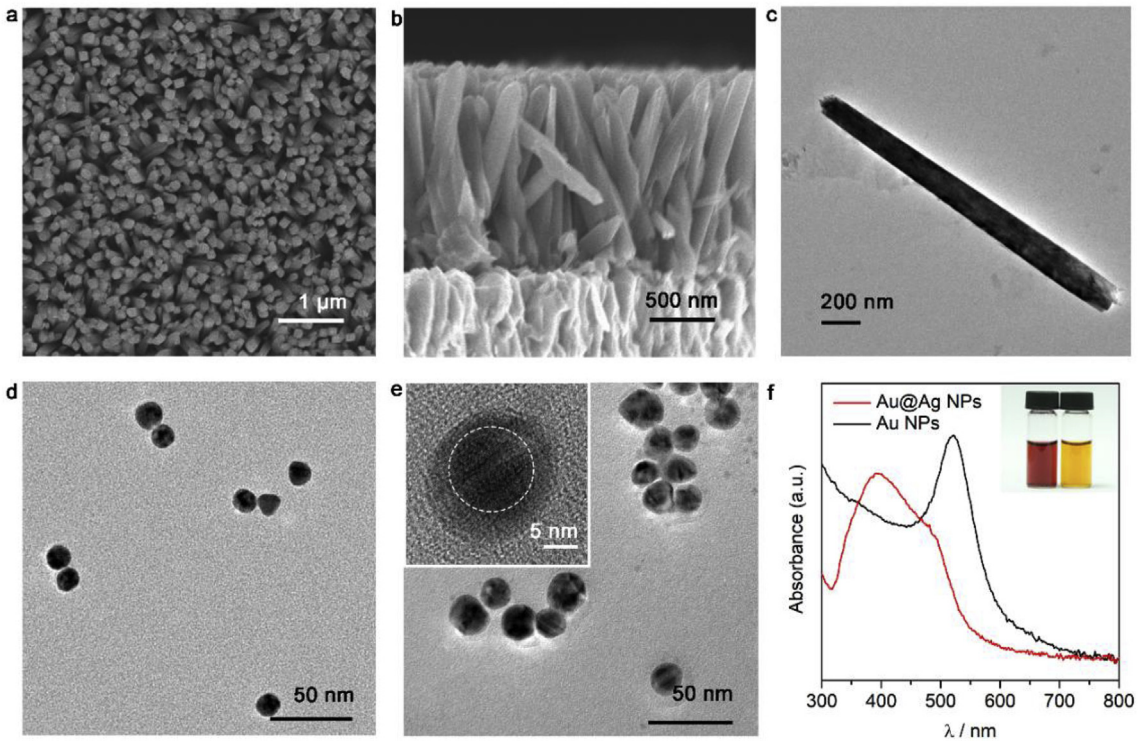

Fig. 1. (a) Top and (b) cross-sectional SEM of TiO_2 NRs; TEM of (c) a single TiO_2 NR, (d) Au NPs, and (e) Au@Ag NPs; Inset of (e) shows a single Au@Ag NP; (f) UV–vis spectra of Au NPs and Au@Ag NPs. Inset of (f) shows the corresponding photographs.

measurements.

2.2. Synthesis of Au@Ag NPs

The fabrication of Au@Ag NPs was according to previous report (Zeng et al., 2018). Specifically, 95 mL water, 5 mL 1% $HAuCl_4$ and 10 mL 38.8 mM sodium citrate were added to 250 mL triple-necked bottle, then the solution was stirred and heated to reflux for 20 min. After that, the solution was stirred and cooled to room temperature and then Au NPs solution was obtained. The Tollens reagent was prepared as follows: adding 1.24 mL ammonia (25%–28%) and 650 μL 3 M NaOH into 6 mL 0.1 M $AgNO_3$, then dilute it to 20 mL by adding water. Add 10 mL Au NPs, 32.2 mL pure water, 3 mL Tollens reagent, and 4.8 mL 10 mM formaldehyde solution to a 100 mL round bottom flask and stir the mixture for 20 min at room temperature to get the Au@Ag NPs solution.

2.3. Preparation of TiO_2 NRs/FTO electrode

FTO conductive glass with the size of 3 × 0.7 cm was ultrasonically cleaned for 5 min in acetone, ethanol and ultra-pure water, respectively and dried with N_2. TiO_2 nanorod arrays were prepared on the FTO slices by hydrothermal method (Liu and Aydil, 2009). The specific process is as follows: 15 mL ultrapure water was mixed with 15 mL hydrochloric acid (37% by weight) in a Teflon-lined stainless autoclave. Following stirring for 2 min, 0.225 mL titanium tetrachloride was added. After stirring for another 2 min, the FTO substrats were slanted into the mixture with the conductive surface downward. After keeping the solution at 150 °C for 2.5 h, the obtained FTO slices were rinsed with deionized water and dried with N_2.

2.4. Assemble of Au@Ag/TiO_2/FTO electrodes

Au@Ag NPs were assembled onto the surface of the prepared TiO_2 NRs/FTO electrodes through the layer-by-layer self-assembly. Specifically, following dipping of the prepared TiO_2 NRs/FTO electrodes into a solution of 2% PDDA containing 0.5 M NaCl for 20 min, the activated electrodes were dipped into the Ag@Au NPs solution for another 20 min to immobilize a monolayer of Ag@Au NPs onto the TiO_2 NRs/ITO electrodes. The electrodes were thoroughly rinsed with ultrapure water after each dipping step. Repeated the above process four times to get satisfactory photocurrent intensity. For the removing of PDDA, the prepared electrodes were annealed in a tubular furnace at 450 °C for 1 h. Before use, the working area of each Au@Ag NPs/TiO_2 NRs/FTO electrode was defined into a geometrical circular area with a diameter of 5 mm.

2.5. Development of DNA biosensor

The hDNA was fixed on the Au@Ag NPs/TiO_2 NRs/FTO electrode via amide bond. Specifically, the Au@Ag NPs/TiO_2 NRs/FTO electrode was incubated in 10% TGA solution at 4 °C overnight. After dried at 60 °C for 40 min, the carboxyl groups modified electrodes were activated in the aqueous solution containing 20 mg/mL EDC and 10 mg/mL NHS at room temperature for 1 h and rinsed with ultrapure water for three times. After that, 25 μL 1.0 μM hDNA was added on the surface of the electrode and kept at 4 °C for 12–16 h. Following blocking with 1 mM MEA at 4 °C for 2 h and rinsing with 0.01 M PBS, the hDNA modified electrode was sequentially incubated with 25 μL tDNA at 37 °C for 1 h and 25 μL 1 μM Hemin for 30 min. After rinsed again with 0.01 M PBS, the electrode was incubated in 1 mM H_2O_2 and 10 mM 4-CN at 37 °C for 30 min. Finally, the photocurrent of the carefully rinsed electrode was measured before and after the addition of H_2O_2 and 4-CN in 0.1 M PBS solution (pH 7.4) containing 0.1 M AA.

3. Results and discussion

3.1. Characterization

TiO_2 NRs were directly grown on FTO conductive glass by the

aforementioned hydrothermal method and the morphology was then revealed by SEM. As shown in Fig. 1a and b, the as-fabricated TiO_2 NRs exhibited a neatly arranged array structure that composed of NRs with about 1.5 μm in length and 150 nm in diameter. For the further investigation of the structure of TiO_2 NRs, the samples were removed from the FTO electrodes by ultrasonication for TEM determination. As illustrated in Fig. 1c, the TEM of a single TiO_2 NR that possessed a rod-like structure with a diameter about 150 nm, which was consistent with the SEM images. The Au@Ag NPs were then prepared by deposition of an Ag shell on the Au NPs and determined by TEM. The reasons for the use of Au@Ag NPs were that Ag NPs have stronger extinction coefficient of the surface plasmon resonance than that of Au NPs with the same size (Cao et al., 2001). As shown in Fig. 1d and e, both of the two NPs appear as quasi-spherical shape with the sizes corresponding to about 13 and 15 nm, respectively. Fig. 1e inset of high-resolution TEM clearly shows the formation of Au@Ag core-shell NP structure. Fig. 1f displays the corresponding UV–vis spectra. As shown, absorption spectrum of the Au NPs with the maximum plasmon absorption peak at ca. 520 nm was observed. By contrast, a broad absorption range from 300 to 550 nm was monitored for Au@Ag NPs, indicating its suitability to be the plasmonic sensitizer under visible light ($\lambda \geq 400$ nm) irradiation. Fig. 1f inset shows the photographs of the Au NPs and Au@Ag NPs solutions. The distinct optical property and the photographs (Fig. 1f) both supported the successful fabrication of the Au@Ag NPs.

The Au@Ag NPs were then coupled onto the TiO_2 NRs matrix and subjected to structural, elemental and optical characterizations. The TiO_2 NRs matrix possessed large surface area with roughness and hence could offer an excellent microenvironment for loading the Au@Ag NPs, as can be observed by Fig. 2a of SEM. In order to further investigate the morphology of Au@Ag NPs modified TiO_2 NRs, TEM was adopted after the samples removed by ultrasonication. More clearly, as shown in Fig. 2b, the Au@Ag NPs were successfully modified onto the TiO_2 NR surface. We further verified this successful immobilization by XPS and the peaks observed at 458, 530, 84 and 367 eV were ascribed to Ti 2p, O 1s, Au 4f and Ag 3d, respectively, as shown in Fig. 2c. Fig. 2d shows the UV–vis diffuse reflectance spectra of the TiO_2 NRs before and after loading Au@Ag NPs. As shown, TiO_2 NRs hardly had any absorption in the visible light range due to its broad band gap excitation, whereas remarkable absorption was observed above 400 nm for Au@Ag NPs/TiO_2 NRs due to the plasmonic sensitization of Au@Ag NPs to TiO_2 NRs. There results indicated the successful preparation of Au@Ag NPs/TiO_2 NRs/FTO electrode and its feasibility for visible-light-driven PEC responses.

3.2. PEC property

To obtain more enriched information on the light-harvesting properties of the electrodes, their PEC performances were then studied by photocurrent action spectra, and recorded by the chronoamperometric I−t curves and I-V curves of the TiO_2/FTO electrode and Au@Ag NPs/TiO_2 NRs/FTO electrode upon visible light illumination. As shown in Fig. 3a, upon irradiation, TiO_2 NRs/FTO electrode showed a smaller photocurrent, whereas the Au@Ag NPs/TiO_2 NRs/FTO electrode exhibited much enhanced and stable photocurrent under no biased potential, suggesting the successful sensitization effect and also the good charge transport within the composite. Such a remarkable response should be attributed to the following reasons: (1) The array structure of TiO_2 NRs could provide high specific area for Au@Ag NPs loading with

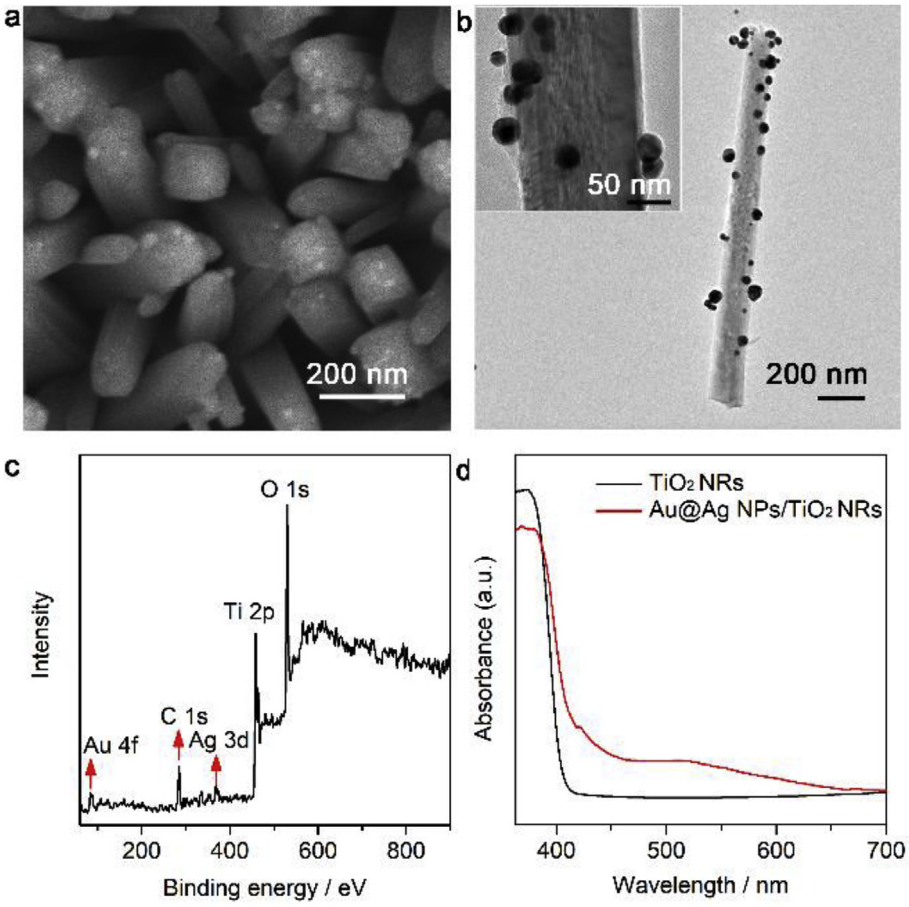

Fig. 2. (a) SEM of Au@Ag NPs/TiO_2 NRs; (b) TEM of a single Au@Ag NPs/TiO_2 NRs; Inset of (b) shows the magnified image; (c) XPS of Au@Ag NPs/TiO_2 NRs; (d) UV–vis diffuse reflectance spectra of TiO_2 NRs and Au@Ag NPs/TiO_2 NRs.

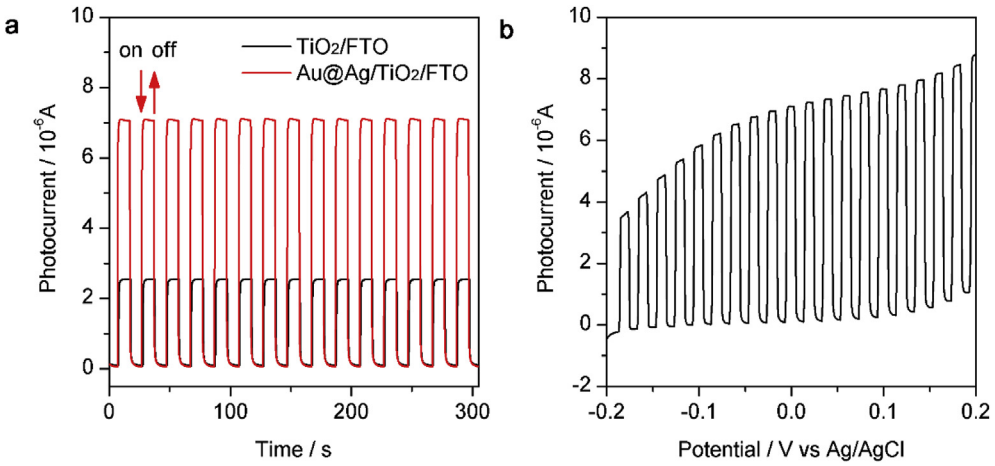

Fig. 3. (a)Time-based photocurrent responses of TiO_2 NRs/FTO electrode and Au@Ag NPs/TiO_2NRs/FTO electrode in a 0.1 M PBS solution (pH 7.4) containing 0.1 M AA at 0 V vs Ag/AgCl under visible light irradiation. (b) I-V curve of Au@Ag NPs/TiO_2 NRs/FTO electrode in 0.1 M PBS solution (pH 7.4) containing 0.1 M AA under visible light irradiation.

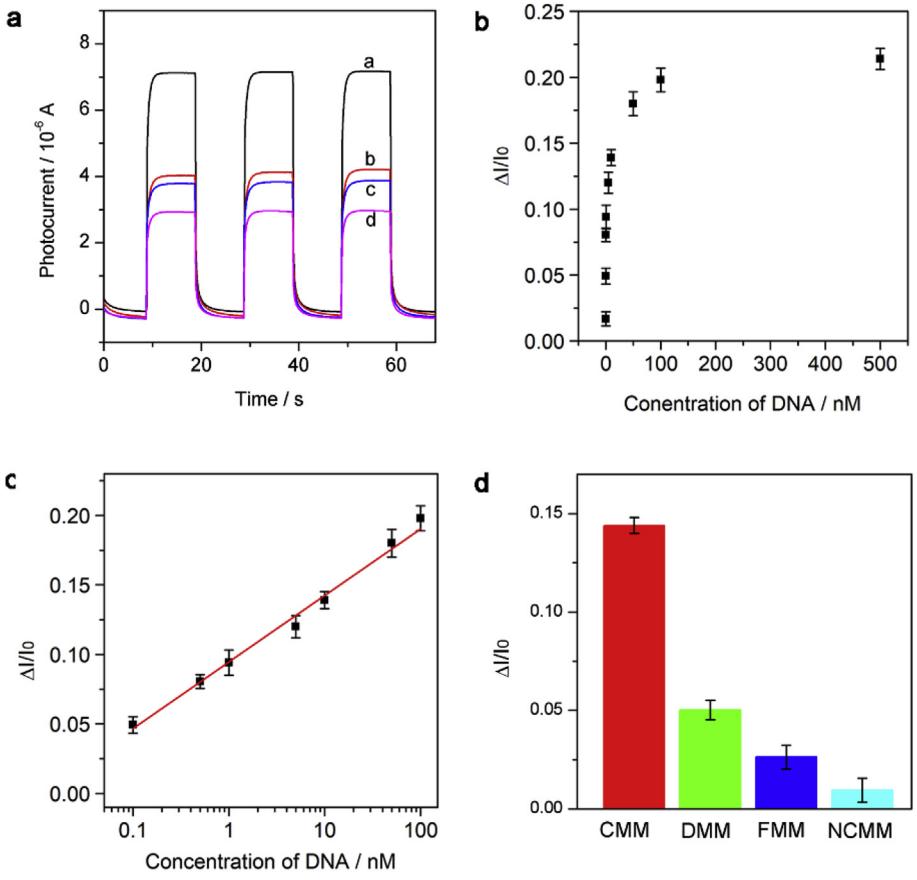

Fig. 4. Performance of Au@Ag NPs/TiO_2NRs/FTO electrode corresponding to DNA determination. (a) Photocurrent response of the Au@Ag NPs/TiO_2 NRs/FTO electrode before (curve a) and after successively modified with hDNA and MEA (curve b), tDNA and Hemin (curve c), H_2O_2 and 4-CN (curve d). (b) Photocurrent response of the electrode corresponding to different concentration of tDNA. (c) The relationship between photocurrent decrease and tDNA concentration increase. (d) Selectivity of the proposed PEC sensor by comparing the detection of 10 nM CMM, DMM, TMM and NCMM. The PEC tests were performed in 0.1 M PBS solution (PH 7.4) containing 0.1 M AA at 0 V vs Ag/AgCl under visible light irradiation.

good contact. (2) Au@Ag NPs modification increased the absorption of Au@Ag NPs/TiO_2 NRs/FTO electrode in the visible range and thus effective stimulating the electron transport between Au@Ag NPs and TiO_2 NRs; (3) On account of the hydrothermal fabrication, the excellent electrical contact between the TiO_2 NRs and the FTO substrate facilitates the efficient charge collection of the FTO. As shown in Fig. 3b, The I-V curves show that Au@Ag NPs/TiO_2 NRs/FTO electrode has a good photoelectric response at 0 V vs Ag/AgCl. In order to eliminate the influence of potential on the determination, 0 V was chosen as the potential for the determination of photocurrent.

3.3. Analytical performance

The prepared electrode was then used to develop the proposed PEC DNA biosensor. Fig. 4a shows the photocurrent response of DNA sensing. After the immobilization of hDNA, the photocurrent of the Au@Ag NPs/TiO_2 NRs/FTO electrode decreased from curve a to curve b, which was due to the steric resistance effect and charge rejection of hDNA that weakened the interaction between the electron donors (AA) and electrodes. Followed by further interaction with tDNA and hemin, as displayed in curve c, the photocurrent exhibited a slight further decrease along with the formation of G-quadruplex-based DNAzyme. When 4-CN and H_2O_2 were added to the DNAzyme-coated Au@Ag NPs/TiO_2 NRs/FTO electrode, an obvious suppression of photocurrent could be observed in curve d. This was because DNAzyme could catalyze the oxidation of 4-CN to form the insoluble and insulating product benao-4-chlorohexadienone, which hindered the interaction between electroactive substances and photoelectrodes. Fig. 4b and c show that there

was a linear relationship between the relative value of tDNA concentration and the magnitude of photocurrent decrease ($\Delta I/I_0$) with a good linear relationship between 0.1 and 100 nM with the detection limit experimentally found as 0.1 nM, where ΔI was defined as the change of photocurrent before (I_0) and after (I_s)the incubation of 4-CN and H_2O_2. In addition, the RSD for six consecutive measurements of 5 nM tDNA at the same batch electrodes was determined as 6.6%, suggesting the good reproducibility. The interference experiments were performed by using DNA with different mismatches as interfering species at the same concentration. As shown in Fig. 4d, only tDNA caused the most obvious decline of the signal, indicating its good selectivity to tDNA. Incidentally, given most DNAzymes suffer from product inhibition and hence exhibit only single-turnover behavior (Zhao et al., 2017), the developed assay is supposed for single-time use.

4. Conclusion

In present work, a novel plasmonic Au@Ag NPs/TiO_2 NRs/FTO heterostructure has been developed and applied for innovative PEC DNA bioanalysis. The as-fabricated photoelectrode possessed excellent PEC performance in terms of good stability, rapid response and high photocurrent generation that originated from the hot electron transfer between Au@Ag NPs and TiO_2 NRs. In the detection, the target-binding-induced conformation change from hDNA to G-quadruplex-based DNAzyme could in situ stimulate the BCP onto the photoelectrode and thereby inhibit the photocurrent generation, and the as-developed biosensor had high sensitivity and selectivity, acceptable reproducibility and good stability. In the range from 0.1 to 100 nM, the depressed photocurrents were in proportion to the concentration of the tDNA. This work features the integration of plasmonic Au@Ag NPs/TiO_2 NRs/FTO heterostructure and target-binding induced BCP in a PEC system for sensitive DNA analysis. The proposed signaling mechanism is expected to provide a novel insight into the design and utilization of new efficient DNAzyme-catalyzed amplification strategies for PEC bioanalysis.

Declaration of interests

The authors declare that they have no known competing financial interests or personal relationships that could have appeared to influence the work reported in this paper.

CRediT authorship contribution statement

Ling Zhang: Data curation, Investigation, Validation. **Xiao-Mei Shi:** Data curation, Investigation, Validation. **Yi-Tong Xu:** Data curation, Investigation, Validation. **Gao-Chao Fan:** Investigation, Validation. **Xiao-Dong Yu:** Conceptualization, Funding acquisition, Project administration, Writing - review & editing. **Yan-Yu Liang:** Conceptualization, Funding acquisition, Project administration, Writing - review & editing. **Wei-Wei Zhao:** Conceptualization, Funding acquisition, Project administration, Writing - review & editing.

Acknowledgements

This work was supported by the National Natural Science Foundation of China (Grant Nos. 21675080, and 21771107) and the Natural Science Foundation of Jiangsu Province, China (Grant Nos. BK20161484, BK20170073), and the Fundamental Research Funds for the Central Universities, China (Grant NO. NE2015003).

References

Cao, Y.W., Jin, R.C., Mirkin, C.A., 2001. J. Am. Chem. Soc. 123, 7961–7962.
Chen, J., Guo, M., Su, H.J., Zhang, J., Liu, L., Huang, H.T., Xie, K.Y., 2018. J. Appl. Electrochem. 48 (10), 1139–1149.
Cui, L., Hu, J., Wang, M., Diao, X.K., Li, C.C., Zhang, C.Y., 2018. Anal. Chem. 90 (19), 11478–11485.
Da, P.M., Li, W.J., Lin, X., Wang, Y.C., Tang, J., Zheng, G.F., 2014. Anal. Chem. 86 (13), 6633–6639.
Ding, L.H., Ma, C., Li, L., Zhang, L.N., Yu, J.H., 2016. J. Electroanal. Chem. 783, 176–181.
Gao, F., Dai, H.T., Pan, H.F., Chen, Y.F., Wang, J.K., Chen, Z.J., 2018. J. Colloid Interface Sci. 513, 693–699.
Ge, L., Wang, W.X., Hou, T., Li, F., 2016. Biosens. Bioelectron. 77, 220–226.
Ghafoor, S., Ata, S., Mahmood, N., Arshad, S.N., 2017. Sci. Rep. 7 (255), 1–10.
Gong, L.S., Dai, H., Zhang, S.P., Lin, Y.Y., 2016. Anal. Chem. 88 (11), 5775–5782.
Kang, Q., Yang, L.X., Chen, Y.F., Luo, S.L., Wen, L.F., Cai, Q.Y., Yao, S.Z., 2010. Anal. Chem. 82 (23), 9749–9754.
Karuturi, S.K., Shen, H.P., Duong, T., Narangari, P.R., Yew, R., Leung, J.W., Catchpole, K., Tan, H.H., Jagadish, C., 2018. ACS Appl. Mater. Interfaces 10 (28), 23766–23773.
Kong, Q.K., Cui, K., Zhang, L.N., Wang, Y.H., Sun, J.L., Ge, S.G., Zhang, Y., Yu, J.H., 2018. Anal. Chem. 90 (19), 11297–11304.
Kulkarni, A.N., Prasad, M.B.R., Pathan, H.M., Patil, R.S., 2016. Appl. Nanosci. 6, 567–574.
Li, H.Y., Bai, H., Lv, Q., Wang, W., Wang, Z.J., Wei, H., Zhang, Q., 2018a. Anal. Chim. Acta 1021, 140–146.
Li, L., Dai, H.T., Feng, L.F., Luo, D., Wang, S.G., Sun, X.W., 2015. Nanoscale Res. Lett. 10, 418.
Li, J., Jin, L.P., Fang, L.L., Zhang, M., Wang, Y.F., Jiang, X.S., Lv, J.G., He, G., Sun, Z.Q., 2018b. Appl. Surf. Sci. 456, 694–700.
Liu, B., Aydil, E.S., 2009. J. Am. Chem. Soc. 131, 3985–3990.
Liu, R.R., Ji, Z.J., Wang, J., Zhang, J.J., 2018b. Microporous Mesoporous Mater. 266, 268–275.
Liu, X.P., Chen, J.S., Mao, C.J., Niu, H.L., Song, J.M., Jin, B.K., 2018a. Biosens. Bioelectron. 116, 23–29.
Nehme, A.S., Haydous, F., Halaoui, L., 2016. J. Phys. Chem. C 120 (9), 4766–4778.
Pathak, P., Podzorski, M., Bahnemann, D., Subramanian, V.R., 2018. J. Phys. Chem. C 122 (25), 13659–13668.
Peng, B., Tang, L., Zeng, G.M., Fang, S.Y., Ouyang, X.L., Long, B.Q., Zhou, Y.Y., Deng, Y.C., Liu, Y.N., Wang, J.J., 2018b. Biosens. Bioelectron. 121, 19–26.
Peng, J.Y., Huang, Q., Zhuge, W.F., Liu, Y.X., Zhang, C.Z., Yang, W., Xiang, G., 2018a. Biosens. Bioelectron. 106, 212–218.
Qileng, A., Wei, J., Lu, N., Liu, W.P., Cai, Y., Chen, M.S., Lei, H.T., Liu, Y.J., 2018. Biosens. Bioelectron. 106, 219–226.
Shen, Q.M., Han, L., Fan, G.C., Zhang, J.R., Jiang, L.P., Zhu, J.J., 2015. Anal. Chem. 87 (9), 4949–4956.
Shi, J.J., Zhu, J.C., Zhao, M., Wang, Y., Yang, P., He, J., 2018a. Talanta 183, 237–244.
Shi, X.M., Wang, C.D., Zhu, Y.C., Zhao, W.W., Yu, X.D., Xu, J.J., Chen, H.Y., 2018b. Anal. Chem. 90 (16), 9687–9690.
Song, J., Wu, S., Xing, P.P., Zhao, Y.Q., Yuan, J.L., 2018a. Anal. Chim. Acta 1001, 24–31.
Song, Z., Fan, G.C., Li, Z.M., Gao, F.X., Luo, X.L., 2018b. Anal. Chem. 90 (18), 10681–10687.
Tu, W.W., Wang, Z.Y., Dai, Z.H., 2018. Trends Anal. Chem. 105, 470–483.
Wang, G.L., Shu, J.X., Dong, Y.M., Wu, X.M., Li, Z.J., 2015. Biosens. Bioelectron. 66, 283–289.
Wang, T., Li, B.R., Pan, J.H., 2018. Colloid. Surf. Physicochem. Eng. Asp. 555, 448–456.
Xu, F.Y., Zhang, J.J., Zhu, B.C., Yu, J.G., Xu, J.S., 2018b. Appl. Catal. B Environ. 230, 194–202.
Xu, L., Jiang, D.S., Zhao, Y., Yan, P.C., Dong, J.T., Qian, J.C., Ao, H.Q., Li, J.W., Yan, C., Li, H.N., 2018a. Dalton Trans. 47, 13353–13359.
Zang, Y., Lei, J.P., Ling, P.H., Ju, H.X., 2015. Anal. Chem. 87 (10), 5430–5436.
Zeng, J.B., Li, M., Liu, A., Feng, F., Zeng, T., Duan, W., Li, M.M., Gong, M.F., Wen, C.Y., Yin, Y.D., 2018. Adv. Funct. Mater. 28 (26) 1800515.
Zhang, G.Y., Shan, D., Dong, H.F., Cosnier, S., Ghanim, K.A.A., Ahmad, Z., Mahboob, S., Zhang, X.J., 2018b. Anal. Chem. 90 (20), 12284–12291.
Zhang, N., Ruan, Y.F., Ma, Z.Y., Zhao, W.W., Xu, J.J., Chen, H.Y., 2016a. Biosens. Bioelectron. 85, 294–299.
Zhang, N., Ruan, Y.F., Zhang, L.B., W.W., Xu, J.J., Chen, H.Y., 2018c. Anal. Chem. 90, 2341–2347.
Zhang, N., Shi, X.M., Guo, H.Q., Zhao, X.Z., Zhao, W.W., Xu, J.J., Chen, H.Y., 2018a. Anal. Chem. 90 (20), 11892–11898.
Zhang, X.J., Zeng, M., Zhang, J.W., Song, A.M., Lin, S.W., 2016b. RSC Adv. 6 (10), 8118–8126.
Zhao, W.W., Ma, Z.Y., Yu, P.P., Dong, X.Y., Xu, J.J., Chen, H.Y., 2012. Anal. Chem. 84 (2), 917–923.
Zhao, W.W., Xu, J.J., Chen, H.Y., 2017. Biosens. Bioelectron. 92, 294–304.
Zhou, G., Meng, H.Y., Cao, Y., Kou, X.J., Duan, S.X., Fan, L.L., Xiao, M., Zhou, F.Z., Li, Z.Z., Xing, Z.P., 2018. J. Ind. Eng. Chem. 64, 188–193.
Zhu, Y.C., Zhang, N., Ruan, Y.F., Zhao, W.W., Xu, J.J., Chen, H.Y., 2016. Anal. Chem. 88 (11), 5626–5630.
Zhuang, J.Y., Lai, W.Q., Xu, M.D., Zhou, Q., Tang, D.P., 2015. ACS Appl. Mater. Interfaces 7, 8330–8338.